IEEE Photonics Journal
An IEEE Photonics Society Publication

Open Access

Control Bandwidth Promotion of Adaptive Fiber-Optics Collimator and Its Application in Coherent Beam Combination

Volume 10, Number 6, December 2018

Guan Huang
Chao Geng
Feng Li
Jiaying Liu
Xinyang Li

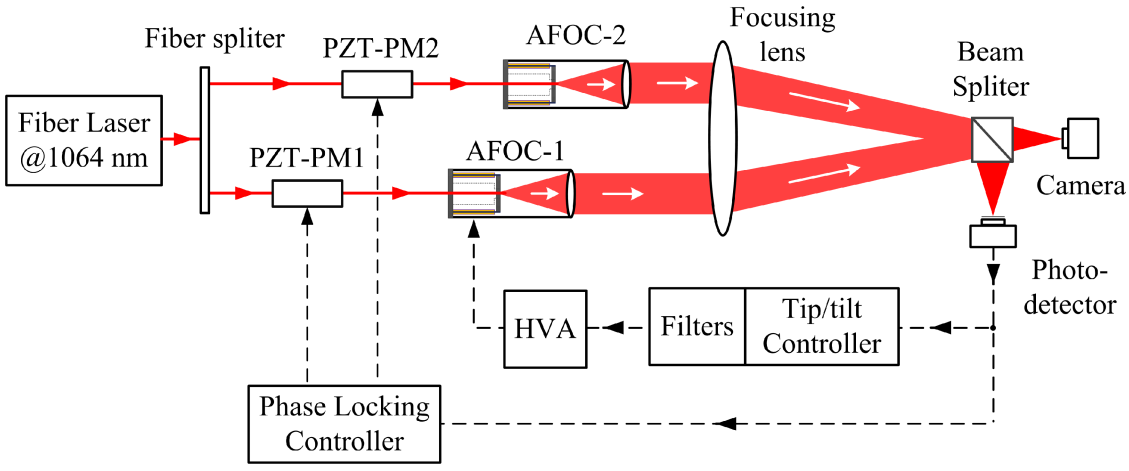

DOI: 10.1109/JPHOT.2018.2876136
1943-0655 © 2018 IEEE

Control Bandwidth Promotion of Adaptive Fiber-Optics Collimator and Its Application in Coherent Beam Combination

Guan Huang,[1,2,3] **Chao Geng**,[1,2] **Feng Li**,[1,2] **Jiaying Liu**,[1,2,3] **and Xinyang Li**[1,2]

[1]Key Laboratory on Adaptive Optics, Chinese Academy of Sciences, Chengdu 610209, China
[2]Institute of Optics and Electronics, Chinese Academy of Sciences, Chengdu 610209, China
[3]University of Chinese Academy of Sciences, Beijing 100049, China

DOI:10.1109/JPHOT.2018.2876136

Manuscript received August 19, 2018; accepted October 11, 2018. Date of publication October 25, 2018; date of current version November 1, 2018. This work was supported in part by the National Natural Science Foundation of China under Grant 61675205, in part by the CAS "Light of West China" program, and in part by the Youth Innovation Promotion Association, CAS. Corresponding author: Chao Geng (e-mail: blast_4006@126.com).

Abstract: Adaptive fiber-optics collimator (AFOC) plays an important role in the coherent beam combining (CBC) systems. To improve the control bandwidth, the frequency characteristics of AFOC are measured, and an accurate transfer function model is established. Through the analysis of this model, we find that the resonance and the inherent response delay are the main limiting factors. To solve these two problems, an active resonance suppression method based on biquad filters and an improved control algorithm named precise-delayed stochastic parallel gradient descent (PD-SPGD) is proposed. The resonance suppression experiment shows that when the frequency is within 10 kHz, the fluctuation in the AFOC's amplitude-frequency characteristic is suppressed within ± 3 dB by the biquad filters, and the phase-frequency characteristic is compensated to be similar to a pure delay element (with inherent response delay of about 88 μs). The two-channel CBC experiment shows that the algorithm's iteration rate increased from 1.6 to 6 kHz and the convergence time decreased from 5.63 to 1.83 ms when the biquad filters and PD-SPGD are used together, which indicate that the AFOC's actual control bandwidth is about 3.1 times higher than before.

Index Terms: Coherent beam combining, adaptive fiber-optics collimator, biquad filters, precise-delayed SPGD algorithm.

1. Introduction

Coherent beam combining (CBC) of fiber lasers is an important research topic in laser communications and beam projection applications [1]–[5]. In recent years, it has been demonstrated that the coherent combined laser beam's quality degrades seriously without tip/tilt control of the fiber laser's wavefronts, even if all the beamlets are phase-locked [3]–[5]. The limited precision of assembling, vibrations of mechanism and atmosphere perturbations usually produce the tip/tilt errors. There are four main tip/tilt control instruments, including liquid crystal spatial light modulator [6], fast steering mirror [7], active segmented mirror [8] and adaptive fiber-optics collimator (AFOC)

[9]–[15]. Compared with other methods, AFOC has the advantages of precise control, small inertia and convenience for packaging. Therefore, it has been widely used in the tip/tilt control loop of the CBC applications and satisfactory results have been achieved [12]–[15].

In such a system, stochastic parallel gradient descent (SPGD) algorithm is usually employed as the control strategy for both phase-locking and tip/tilt control. In the previous demonstrated CBC system, piezoelectric-ring phase-modulator (PZT PM) and LiNbO3 PM are usually employed as the phase-locking actuator. They both provides extremely high operational frequency bandwidth and the maximum iteration rate of the SPGD algorithm that can be supported are dozens of kHz and even hundreds of kHz respectively [12]–[15]. However, the iteration rates of SPGD algorithm in the AFOC-based tip/tilt control loop mentioned are within 3 kHz [12]–[15], which is barely compatible with the high correction bandwidth required for tip/tilt control in the atmospheric environment, for the characteristic frequency of the turbulence-induced tip/tilt aberrations is close to 100 Hz [16].

There are two main reasons for the limited iteration rate. Firstly, as a typical bimorph-based device, the operational frequency bandwidth of AFOC is restricted with resonances, where the amplitude of the induced deviation can increase significantly up to a level where the device will be broken [9]. Secondly, our recent research [17] shows that there exists an inherent response delay in the tip/tilt control loop, which could lead to the fuzzy gradient estimation result during the high-speed iteration process of SPGD. For the first problem, a passive damping structure have been added to the AFOC by L. Beresnev *et al*. [9], where the viscouselastic materials is installed in contact with the actuator's moving parts. However, this method will decrease the deviation range of AFOC by almost two times [9], [10]. Therefore, it has limited effect on the devices which requiring large offsets. For the second problem, our group proposed an improved control algorithm named precise-delayed SPGD (PD-SPGD) recently [17]. It has been successfully applied in the adaptive single-mode fiber coupling system, where a pint-sized AFOC with relatively flat amplitude-frequency characteristic is employed as the actuator, and the iteration rate increases from 3 kHz to 8 kHz with PD-SPGD. However, this algorithm has not been tried in CBC systems where the standard-sized AFOC with greater driving force and offset is usually used, which is more susceptible to the resonance.

In this paper, a more convenient and efficient active resonance suppression method based on biquad filters [18] is proposed, which can make the AFOC's amplitude frequency characteristic almost completely flat when the frequency is within 10 kHz, and it will not decrease the deviation range. In addition, the PD-SPGD algorithm is first applied to the tip/tilt control loop of the CBC system to compensate for the inherent response delay of about 88 μs. The rest of this paper is organized as follows. Test experiment of AFOC's frequency characteristics and the fitted transfer function model is shown in Section 2. In Section 3, the influence of AFOC's frequency characteristic on the SPGD algorithm's convergence performance is analyzed, and the principle of the active resonance suppression method based on biquad filters and the PD-SPGD algorithm is proposed. In Section 4, a resonance suppression experiment and a two-channel CBC experiment are conducted to verify the effectiveness of both two methods mentioned above.

2. Current Situation

2.1 Frequency Characteristics of AFOC

Fig. 1 shows the structural scheme of frequency characteristics measurement system. The collimated laser beam from AFOC is focused and then reaches on the photosensitive area of the position sensitive detector (PSD) through a microscope objective. Chirp signals generated by the testing instrument are amplified by high-voltage amplifier (HVA), and then applied to AFOC to produce the corresponding displacement on the fiber tip. This displacement will eventually be converted to the offset of the focal spot on the PSD, and then transfers to the testing instrument. The wavelength of the fiber laser used here is $\lambda = 1064$ nm, the beam diameter is $D = 28$ mm, the focal length of the collimate lens and the focusing lens is $f_1 = 150$ mm and $f_2 = 2$ m respectively.

Here, the measured device is labeled as AFOC-1, and the test results of its *X*-direction are shown in Fig. 2. The amplitude-frequency characteristic shows the first-order resonance peak

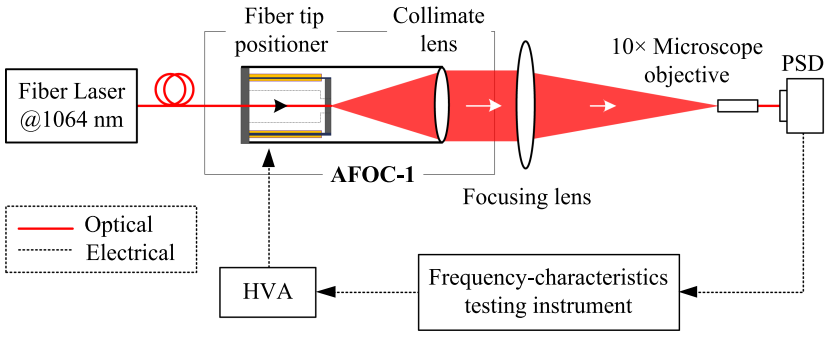

Fig. 1. Structural scheme of frequency characteristics measurement system of AFOC.

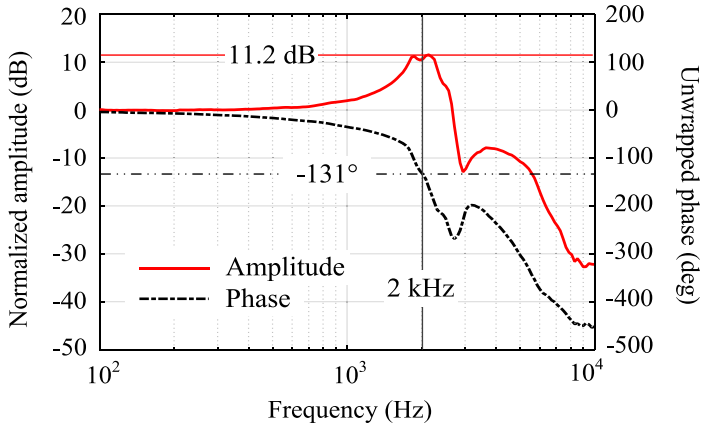

Fig. 2. Frequency characteristics measurement result of *X*-direction of AFOC-1.

appears around 2 kHz, and the induced deviation is amplified by about 11.2 dB. The phase-frequency characteristic indicates that the induced deviation lagged about 131° when the frequency is 2 kHz. The analysis presented below shows that these two characteristics together determine the convergence performance of SPGD.

2.2 Transfer Function Model

In the traditional adaptive optics, the frequency characteristics of the piezoelectric fast steering mirror (PFSM) can be represented by the combination of several biquad resonance elements [18]. Due to the piezoelectric ceramics are also used as driving units in PFSM and AFOC (bimorph used in the AFOC is an assembly of two piezoelectric ceramics cemented together [9]), we try to use this combination model to fit the frequency characteristics of AFOC. Here, $F_{\mathrm{AFOC}}(s)$ and $F_{\mathrm{CM}}(s)$ are used to represent the frequency characteristics of the measured result and the combination model. The form of $F_{\mathrm{CM}}(s)$ is shown in formula 1:

$$F_{\mathrm{CM}}(s) = F_1(s) \cdot F_2(s) \cdot F_3(s) \ldots \tag{1}$$

Where each of these biquad resonance elements is shown in formula 2:

$$F_k(s) = \frac{s^2/\omega_{zk}^2 + 2\xi_{zk}s/\omega_{zk} + 1}{s^2/\omega_{pk}^2 + 2\xi_{pk}s/\omega_{pk} + 1} = G_{pk}(s) \cdot G_{zk}(s) \tag{2}$$

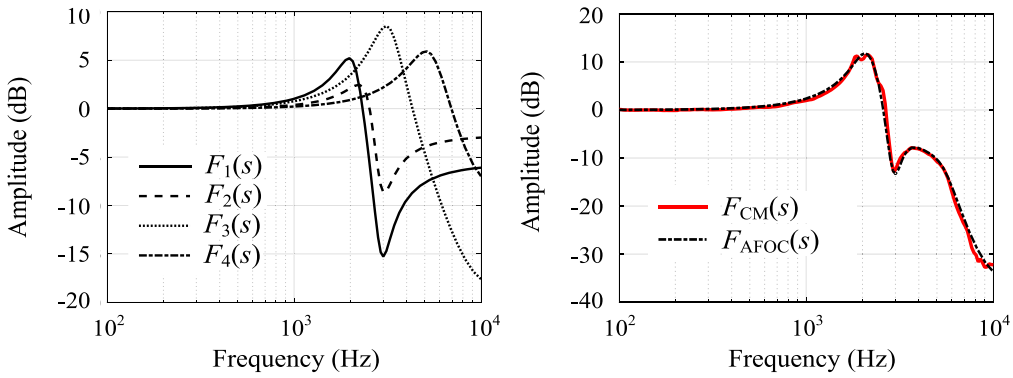

Fig. 3. The fitting results for AFOC's amplitude-frequency characteristic.

TABLE 1
Fitting Parameters Used in the Combination Model

Elements	ω_z (kHz)	ξ_z	ω_p (kHz)	ξ_p
$F_1(s)$	2.11	0.15	2.93	0.09
$F_2(s)$	2.55	0.12	2.93	0.10
$F_3(s)$	3.23	0.19	9.00	0.49
$F_4(s)$	5.42	0.24	9.00	0.49

Where ξ_{zk} and ξ_{pk} are usually called damping ratio, ω_{zk} and ω_{pk} are usually called natural resonance frequency. $G_{pk}(s)$ is the typical second order oscillation element and $G_{zk}(s)$ is the inverse of it, which is commonly known as second order differentiation element. The combination model $F_{CM}(s)$ is first used to fit the amplitude-frequency characteristic of AFOC, and we find that good matching can be obtained by the $F_{CM}(s)$ with four biquad resonance elements $F_k(s)$. The amplitude-frequency characteristics of $F_k(s)$, $F_{CM}(s)$ and $F_{AFOC}(s)$ are shown in Fig. 3, and the fitting parameters are shown in Table 1.

The phase-frequency characteristics of $F_{AFOC}(s)$ and $F_{CM}(s)$ are shown in Fig. 4. We find that there exists a pure delay element $e^{-(8.8e-05)s}$ between the two. The phase-frequency characteristics are well fitted when $e^{-(8.8e-05)s}$ is added in $F_{CM}(s)$.

In conclusion, the transfer function model of AFOC can be represented by the combination model $F_{CM}(s)$ with four biquad oscillation elements and an inherent response delay element $e^{-(8.8e-05)s}$, as shown in formula 3. Here $F_{AFOC}'(s)$ is used to represent the final fitting model, and the fitting errors between $F_{AFOC}'(s)$ and $F_{AFOC}(s)$ are within 3 dB and 30° respectively when the frequency is within 10 kHz, as shown in Fig. 5.

$$F'_{AFOC}(s) = F_{CM}(s) \cdot e^{-(8.8e-5)s} = F_1(s) \cdot F_2(s) \cdot F_3(s) \cdot F_4(s) \cdot e^{-(8.8e-5)s} \tag{3}$$

3. Problems and Their Solution

3.1 Problems

In the CBC experiments, SPGD algorithm is usually used to calculate the appropriate control voltages for AFOCs to realize the accurate adaptive correction of the tip/tilt errors, where the

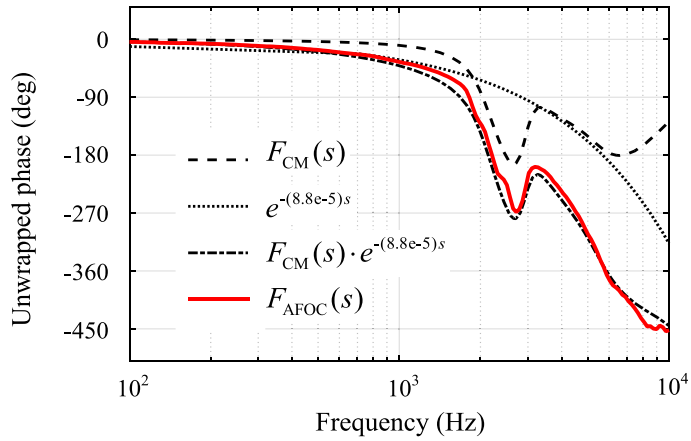

Fig. 4. The fitting results for AFOC's phase-frequency characteristic.

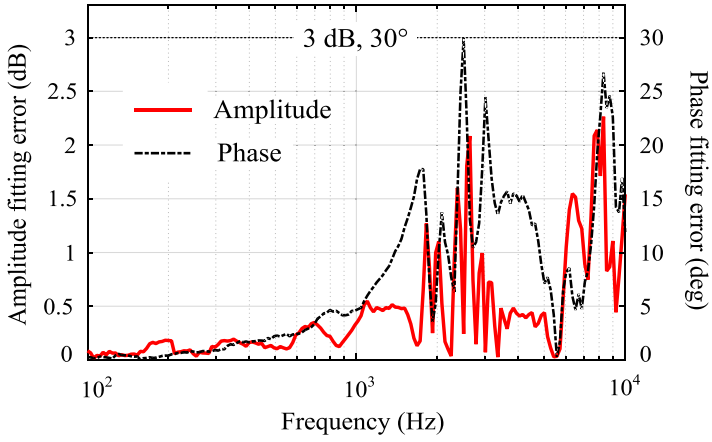

Fig. 5. Fitting errors of the AFOC's frequency characteristics.

N-dimension control voltages $\mathbf{U}^{(n)} = \{u_1^{(n)}, u_2^{(n)}, \ldots, u_N^{(n)}\}$ is updated by formula 4:

$$\mathbf{U}^{(n+1)} = \mathbf{U}^{(n)} + \gamma \Delta \mathbf{U}^{(n)} \left[J_+^{(n)} - J_-^{(n)} \right] \tag{4}$$

Where γ is the gain coefficient and $\Delta\mathbf{U}^{(n)} = \{\delta u_1^{(n)}, \delta u_2^{(n)}, \ldots, \delta u_N^{(n)}\}$ is a set of *N*-dimension small-amplitude random control voltage changes, denoted as perturbations. The perturbations in the form $\mathbf{U}^{(n)} + \Delta\mathbf{U}^{(n)}$ (positive) and $\mathbf{U}^{(n)} - \Delta\mathbf{U}^{(n)}$ (negative) are applied between two sequential updates of the control voltages. They are responsible for the corresponding changes in the performance metrics ($J_+^{(n)}$ and $J_-^{(n)}$), so that the current optimization gradient direction can be detected. Obviously, the responses of AFOCs to these perturbations determine the convergence performance of SPGD.

For further analysis, we simulated a set of such perturbations with unit amplitude, hereafter referred to as $\mathbf{U}_{dith}$. The AFOC's responses generated by the transfer function $F_{\mathrm{CM}}(s)$, $e^{-(8.8\mathrm{e}-05)s}$ and $F_{\mathrm{AFOC}}{}'(s)$ are discussed separately, and they are expressed as $\mathbf{U}_{cm}$, $\mathbf{U}_{delay}$ and $\mathbf{U}_{afoc}$. The simulation results are as follows.

Fig. 6(a) shows $\mathbf{U}_{dith}$ and $\mathbf{U}_{cm}$ with the iteration rate of 500 Hz. We can find that there are oscillations in $\mathbf{U}_{cm}$ after each step changes of the input perturbations $\mathbf{U}_{dith}$. The frequency spectrums in Fig. 6(b) indicates that the high frequency components in $\mathbf{U}_{dith}$ (from 1 kHz to 3 kHz) are amplified by the resonance around 2 kHz, which is answerable to the oscillations in the time

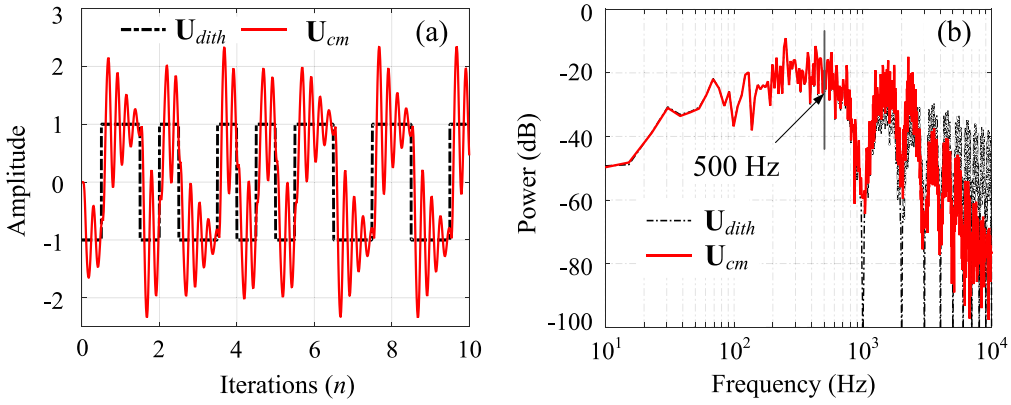

Fig. 6. (a) Perturbations $\mathbf{U}_{dith}$ and the response $\mathbf{U}_{cm}$; (b) frequency spectrums.

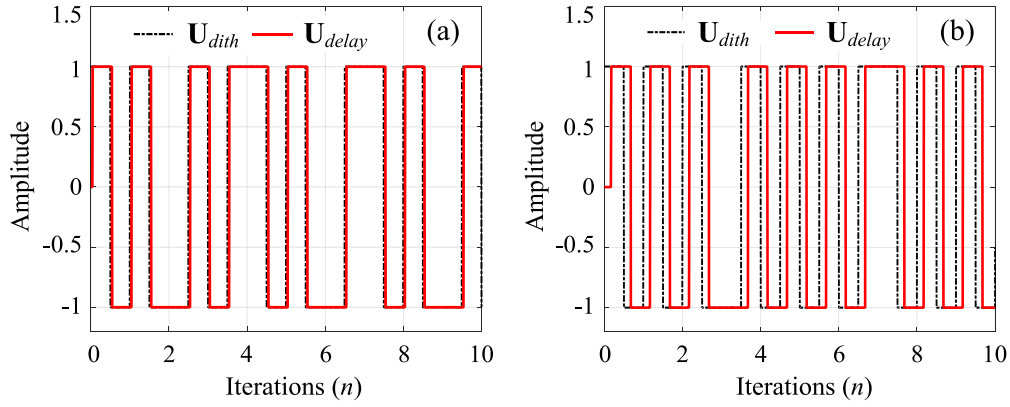

Fig. 7. Perturbations $\mathbf{U}_{dith}$ and the response $\mathbf{U}_{delay}$ with the iteration rate of 500 Hz (a) and 2 kHz (b).

domain. It can be predicted that when the iteration rate of SPGD algorithm keeps increasing, the oscillations in $\mathbf{U}_{cm}$ will become more intense, and the convergence performance of SPGD algorithm will gradually decrease.

Fig. 7 shows $\mathbf{U}_{dith}$ and $\mathbf{U}_{delay}$ with the iteration rate of 500 Hz and 2 kHz respectively. It can be seen that the phase-lagging between $\mathbf{U}_{dith}$ and $\mathbf{U}_{delay}$ starts growing when the iteration rate is increased to 2 kHz. The inherent response delay (to hereafter refer to as τ_{resp}) caused by $e^{-(8.8e-05)s}$ is about 88 μs. Therefore, when the iteration rate is beyond 5.7 kHz, the response of $\mathbf{U}_{dith}$ will be partial reversed. This will cause a completely untrusted gradient detection result.

In order to compare the influence of both oscillations caused by the resonance and phase-lagging caused by τ_{resp}, we calculated the Pearson's correlation coefficients between the perturbations $\mathbf{U}_{dith}$ and corresponding responses $\mathbf{U}_{cm}$, $\mathbf{U}_{delay}$ and $\mathbf{U}_{afoc}$ under a series of iteration rates. These three calculated correlation coefficients are represented as ρ_1, ρ_2 and ρ_3. The results are shown in Fig. 8.

It can be seen that the overall trend of both curves ρ_1 and ρ_2 is decreased with the increase of iteration rate. The curve ρ_3 represent the influence of both resonance and τ_{resp} on the AFOC's response to $\mathbf{U}_{dith}$. This value is smaller than ρ_1 and ρ_2 at any given iteration rate. When the iteration rate is 2 kHz and τ_{resp} is not considered, the perturbations $\mathbf{U}_{dith}$ and the corresponding response $\mathbf{U}_{cm}$ are still relevant ($\rho_1 = 0.335$). However, when τ_{resp} is considered, they are completely irrelevant ($\rho_3 = -0.051$). Obviously, the SPGD algorithm is bound to diverge in this case. It can be concluded that resonance and inherent response delay τ_{resp} together determines the convergence performance

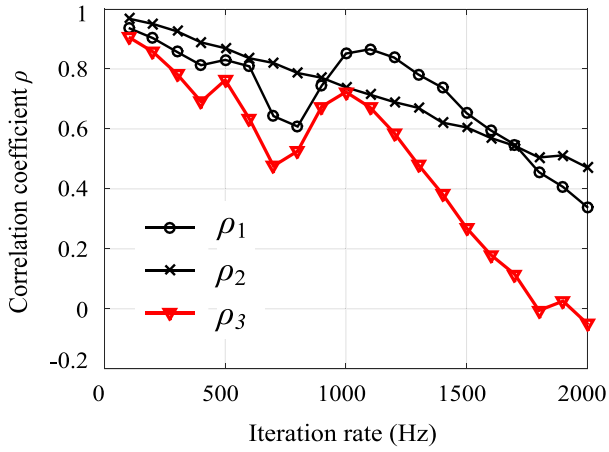

Fig. 8. Correlation coefficients of the perturbations and the corresponding responses of AFOC.

of SPGD, and the effect of both these two will be extended gradually with the increase of the iteration rate. Therefore, we need to solve both problems simultaneously.

3.2 Solution I: Active Resonance Suppression

As shown in Section 2.2, the transfer function model of AFOC can be represented by the combination model $F_{CM}(s)$ with four biquad oscillation elements and an inherent response delay element $e^{-(8.8e-05)s}$. Therefore, for each biquad oscillation element $F_k(s)$, if there exists a biquad filter $F_{BFk}(s)$ with the exact opposite frequency characteristics of $F_k(s)$, then the resonance composition caused by this oscillation element can be compensated by cascading $F_{BFk}(s)$. The detailed form of $F_{BFk}(s)$ is shown in formula 5:

$$F_{BFk}(s) = \frac{1}{F_k(s)} = \left[\frac{s^2/\omega_{pk}^2 + 2\xi_{pk}s/\omega_{pk} + 1}{s^2/\omega_{zk}^2 + 2\xi_{zk}s/\omega_{zk} + 1}\right] \tag{5}$$

Furthermore, if there exists such four biquad filters $F_{BFk}(s)$ with the exact opposite frequency characteristics of each $F_k(s)$, then the transfer function of AFOC can be compensated to a pure delay system. Here, $F_{BF}^m(s)$ is used to represent the combination of the former m biquad filters, as shown in formula 6. The frequency characteristics of $F_{BF}^m(s)$ and the compensated system $F_{AFOC}(s) \cdot F_{BF}^m(s)$ obtained through simulations are shown in Fig. 9.

$$F_{BF}^m(s) = \prod_{k=1}^{m} F_{BFk}(s) \tag{6}$$

Fig. 9(a) shows the amplitude-frequency characteristic of the combination of the former m biquad filters, and Fig. 9(b) shows the amplitude-frequency characteristic of the AFOC after being compensated by such filters. Fig. 9(b) indicates that as the parameter m (the number of filters used) increases, the resonance peak of the compensated system gradually flattens out and moves toward the high frequency direction. Fig. 9(c) and Fig. 9(d) shows the corresponding phase-frequency characteristic. In Fig. 9(d), the curve tends to be linear as m increases. It indicates that the compensated system gradually tends to a pure delay system with an inherent response delay of a fixed value.

3.3 Solution II: Inherent Response Delay Compensation

Due to the inherent response delay in the compensated system is an approximate constant value, it can be compensated by setting a precise time delay between the disturbed voltages and the

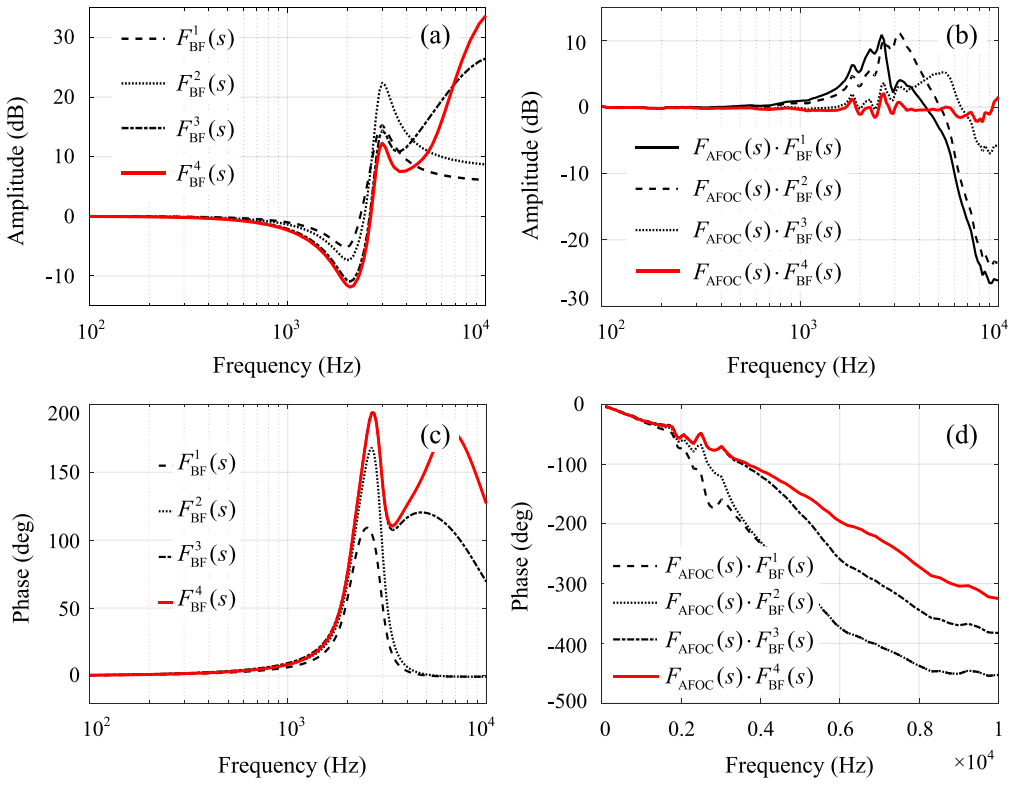

Fig. 9. Amplitude-frequency characteristic of the biquad filters (a) and the compensated system (b); Phase-frequency characteristic of the biquad filters (c) and the compensated system (d).

performance metrics in advance. This idea is originated from delayed-SPGD algorithm (D-SPGD), which was proposed by T. Weyrauch *et al.* and had been successfully used to compensate for the total time delay caused by the optical wave propagation in CBC experiments [14]. In previous studies, we found that the D-SPGD algorithm could easily result in the inadequate compensation or over compensation when dealing with the inherent response delay of AFOC's control loop. We need to set a controllable time delay in a more careful and precise manner [17].

In the proposed PD-SPGD algorithm, the sampling rate of the performance metrics is set to many times (hereafter refer to as *K*) of the iteration rate, and these metrics captured during the several historical iterations (hereafter refer to as *M*) are recorded in the controller memory. Therefore, we can get a sequence of performance metrics at each iteration (n), represented here as $J_0^{(n)}, J_1^{(n)}, \ldots, J_{MK}^{(n)}$. Then, we can take a specific selection from these metrics to perform the gradient estimation, and update the control voltages from $\mathbf{U}^{(n)}$ to $\mathbf{U}^{(n+1)}$, as shown in following formula:

$$\mathbf{U}^{(n+1)} = \mathbf{U}^{(n)} + \gamma \Delta \mathbf{U}^{(n-\Delta n)} \left[J_p^{(n)} - J_{p+K/2}^{(n)} \right] \tag{7}$$

$$\Delta n = \text{int}\left\langle \frac{\tau_{resp} + \tau_{spgd}/4}{\tau_{spgd}} \right\rangle, \quad p = \text{int}\left\langle K \frac{\tau_{resp} + \tau_{spgd}/4}{\tau_{spgd}} \right\rangle \tag{8}$$

Here, $\Delta \mathbf{U}^{(n-\Delta n)}$ is the random perturbations disturbed in the iteration (n-Δn). $J_p^{(n)}$ and $J_{p+K/2}^{(n)}$ are the selected metrics that corresponding to the disturbed voltages $\mathbf{U}^{(n-\Delta n)} + \Delta \mathbf{U}^{(n-\Delta n)}$ and $\mathbf{U}^{(n-\Delta n)} - \Delta \mathbf{U}^{(n-\Delta n)}$. The newly added two parameters Δn and p are defined as the integral-delay parameter and the precise-delay parameter respectively. The operator "int $< >$" used in formula 8 denotes integer conversion. In addition, to ensure that all these metrics are sampled during the period between the disturbed voltages change and the corresponding metrics response, parameter *M* is

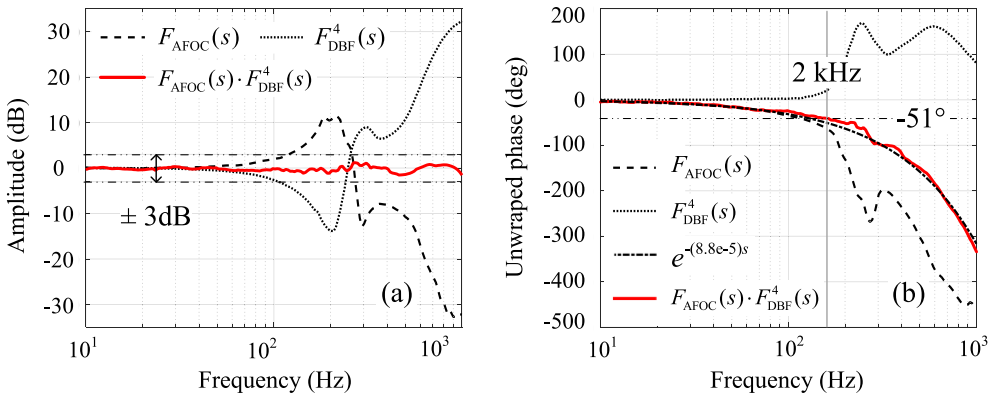

Fig. 10. Amplitude-frequency characteristic (a) and phase-frequency characteristic (b) of the cascaded digital biquad filters and the compensated system.

usually set to $\Delta n + 1$. Parameter K is usually set to an integer bigger than 10, to provide enough compensation accuracy of PD-SPGD algorithm.

4. Experiment

4.1 Resonance Suppression Experiment

In this experiment, the measurement system described in Fig. 1 is used to test the effectiveness of the active resonance suppression method. Here, a Xilinx Spartan 6 series FPGA chip with analog input/output cards are used to implement four cascaded digital biquad filters $F_{DBF}{}^4(s)$ that are expected to have the same frequency characteristics of $F_{BF}{}^4(s)$. The filters are inserted between the controller and HVA. The tested frequency characteristics of the filters $F_{DBF}{}^4(s)$ and the compensated system $F_{AFOC}(s)\cdot F_{DBF}{}^4(s)$ are shown in Fig. 10.

Fig. 10(a) shows that when the frequency is within 10 kHz, the amplitude-frequency characteristic of the compensated system $F_{AFOC}(s)\cdot F_{DBF}{}^4(s)$ is almost completely flattened, and its fluctuations are suppressed in $\pm$3 dB. In Fig. 10(b), it can be seen that the phase-lagging of $F_{AFOC}(s)\cdot F_{DBF}{}^4(s)$ is compensated to $-51°$ at 2 kHz, and the characteristic curve also almost overlap with the inherent response delay module $e^{-(8.8e-05)s}$. The results indicate that the compensated system $F_{AFOC}(s)\cdot F_{DBF}{}^4(s)$ has been successfully transformed into a pure delay system with inherent response delay of about 88 μs.

4.2 Two-Channel CBC Experiment

A two-channel CBC experiment using active resonance suppression method and PD-SPGD algorithm is conducted. The structural scheme is shown in Fig. 11, which is basically the same as the CBC system we represented before [4]. The special part in this structure is that the tip/tilt control voltages is only applied to the X-direction of AFOC-1 (the direction which we measured and filtered before), and the filters $F_{DBF}{}^4(s)$ are inserted between the controller and HVA. In addition, the laser beam emitted by AFOC-2 is well overlapped with the pinhole placed in front of the photodetector. The wavelength of the fiber laser is 1064 nm, the beam diameter is 28 mm, and the focal length of the focusing lens is 2 m.

Here, SPGD algorithm with iteration rate of 20 kHz and 1.6 kHz is employed as the control strategy for phase locking and tip/tilt control separately. The iteration curve of the normalized performance metrics J and the long-exposure far-field intensity distributions acquired by the camera are shown in Fig. 12. The operation status contains four different steps: (I) two control loops didn't perform any correction; (II) only the phase locking control was performed; (III) both phase locking and tip/tilt

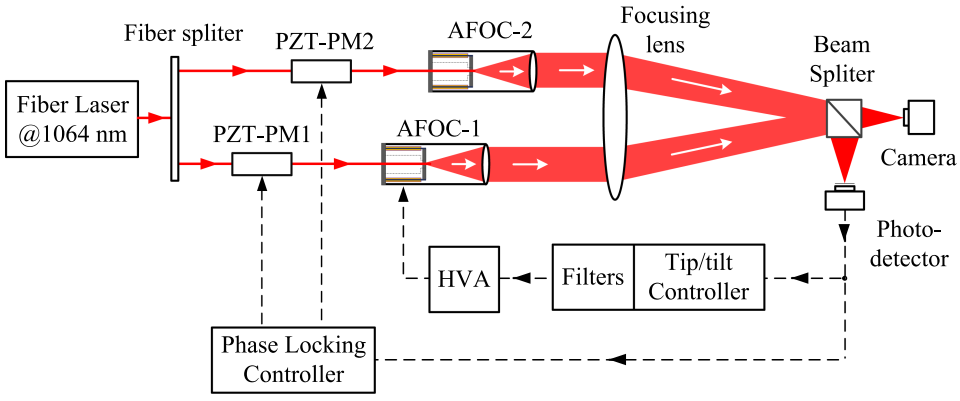

Fig. 11. Structural scheme of the two-channel CBC experiment.

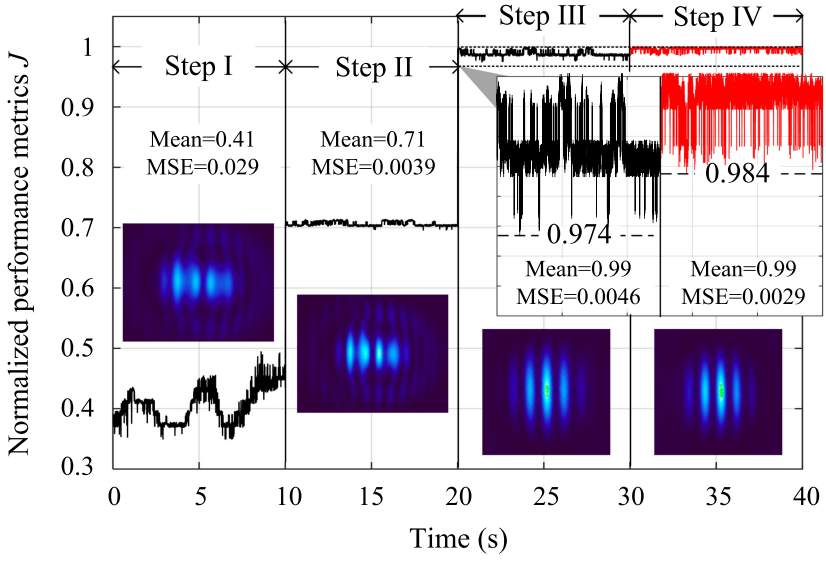

Fig. 12. Structural scheme of the two-channel CBC experiment.

control were performed, whereas the filters were not used; (IV) filters were used on the basis of the precious step.

By means of only correcting piston errors with PZT-PMs in step (II), the average of J was increased by 73%. When the static tip/tilt errors were corrected in step (III), the average of J was increased by 39%. When the filters were used in step (IV), the average of J did not show a significantly change, and there was no clearly difference in the corresponding long-exposure far-field intensity distributions. However, the corresponding MSE and the dithering range of J were decreased by 37% and 38% in step (IV). This result indicates that the stability of the closed-loop performance metrics J has improved by the biquad filters.

In a follow-up experiment, the phase locking control and the filters is always performed, and the PD-SPGD algorithm is used to compensate for the inherent response delay of about 88 μs in the tip/tilt control loop [17]. The iteration rate of PD-SPGD algorithm set up here is 6 kHz and the sampling rate is 60 kHz, thus $\tau_{spgd} = 166.7$ μs and $K = 10$. To compensate for 88 μs response delay, we can figure that $\Delta n = 1$ and $p = 8$ (the closest integer number to 129.7/166.7 and 1297/166.7). Another key parameter M is equal to 2 in this case, so the recorded metrics can be

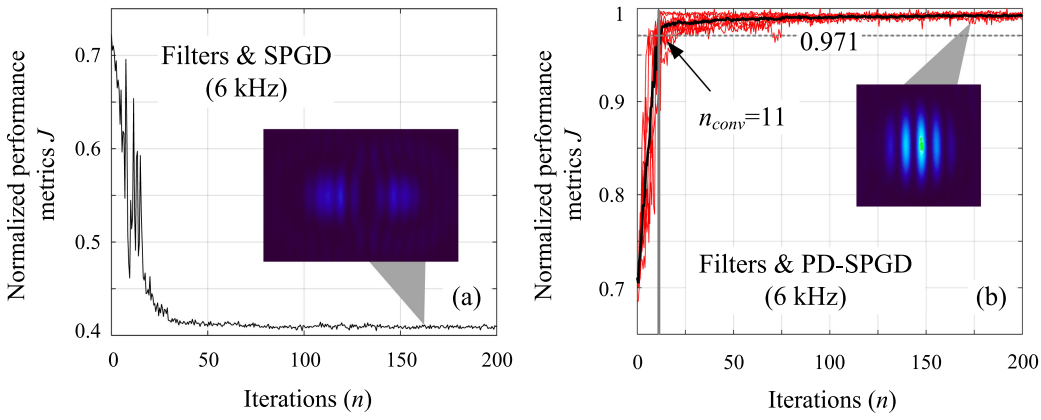

Fig. 13. Iteration curve of normalized performance metrics J of SPGD and PD-SPGD with iteration rate of 6 kHz.

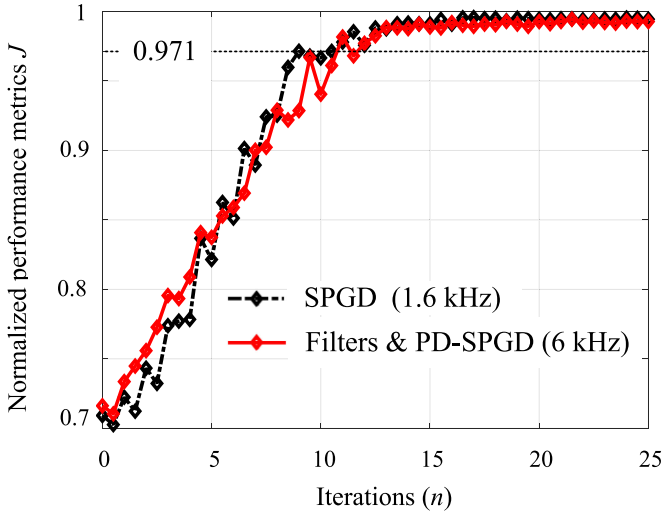

Fig. 14. Averaged iteration curve of the SPGD and the PD-SPGD with iteration rate of 1.6 kHz and 6 kHz.

expressed as $J_0^{(n)}, J_1^{(n)}, \ldots, J_{20}^{(n)}$ at each iteration (n), and the selected metrics of PD-SPGD are $J_8^{(n)}$ and $J_{13}^{(n)}$. Convergence iteration n_{conv} is used to evaluate the corrective performance, which is equal to the iterations needed for the normalized performance metrics J to reach the 90% of the whole convergence process, and it is about 0.971 in this experiment.

As shown in Fig. 13, the SPGD algorithm (with the filters) diverged at the iteration rate of 6 kHz, whereas the PD-SPGD algorithm (with the filters) converged and n_{conv} can be counted as 11 by ten sets of data. This result indicate that the inherent response delay becomes the main reason for the limited iteration rate of SPGD when the resonance is suppressed, and the iteration rate is successively increased to 6 kHz when the inherent response delay is compensated by the PD-SPGD. However, as a typical blind optimization algorithm, the higher control bandwidth of SPGD depends on the shorter convergence time, which is determined not only by the iteration rate, but also by the iterations required to converge. Our previous experiments show that the PD-SPGD algorithm (with appropriate parameter setting) can improve the iteration rate without interfering too much with the convergence iteration n_{conv}. This conclusion is reconfirmed in Fig. 14, which shows

the averaged iteration cure of the SPGD algorithm and the PD-SPGD algorithm with iteration rate of 1.6 kHz and 6 kHz. Each curve is obtained by averaging ten sets of data, and the convergence iteration n_{conv} can be counted as 9 and 11. Therefore, the actual convergence time is 5.63 ms and 1.83 ms for SPGD and PD-SPGD algorithm respectively. Results from this experiment indicate that the actual control bandwidth of AFOC will be 3.1 times higher than before by the biquad filters and the PD-SPGD algorithm.

5. Conclusions

In this paper, we have demonstrated a novel adaptive optical device, AFOC, which is widely used in the tip/tilt control loop of the CBC system. A frequency characteristics measurement experiment of AFOC is firstly conducted, and the accurate transfer function model is established. By analysis of this model, we find that the oscillations caused by the resonance and phase-lagging caused by the inherent response delay τ_{resp} together determine the SPGD algorithm's performance. To solve these two problems, an active resonance suppression method based on biquad filters and an improved control algorithm named PD-SPGD is proposed. The resonance suppression experiment tells that the amplitude-frequency characteristic of AFOC has been completely flattened by the biquad filters, and its fluctuations are suppressed in $\pm$3 dB when the frequency is within 10 kHz. At the same time, the AFOC's phase-frequency characteristic is also compensated to be similar to a pure delay element (with inherent response delay of about 88 μs). At the end, a two-channel CBC experiment is conducted. The result shows that the algorithm's iteration rate increased from 1.6 kHz to 6 kHz and the actual convergence time decreased from 5.63 ms to 1.83 ms when the filters and the PD-SPGD algorithm are performed simultaneously, which indicate that the actual control bandwidth has been 3.1 times higher than before. Obviously, the AFOCs with higher control bandwidth give the CBC system the ability to cope with stronger atmospheric turbulence. In the experiments, we also find that the high frequency noise in the control loop will be easily amplified by the biquad filters. As a practical matter, another low pass filter is needed to set between the HVA and the biquad filters, to suppress the high frequency noise that independent of the control voltages in the control loop.

References

[1] T. Fan, "Laser beam combining for high-power, high-radiance sources," *IEEE J. Sel. Topics Quantum Electron.*, vol. 11, no. 3, pp. 567–577, May 2005.

[2] S. Mcnaught *et al.*, "Scalable coherent combining of kilowatt fiber amplifiers into a 2.4-kw beam," *IEEE J. Sel. Topics Quantum Electron.*, vol. 20, no. 5, pp. 174–181, Sep. 2014.

[3] T. Weyrauch *et al.*, "Deep turbulence effects mitigation with coherent combining of 21 laser beams over 7 km," *Opt. Lett.*, vol. 41, no. 4, pp. 840–843, Feb. 2016.

[4] C. Geng, W. Luo, Y. Tan, H. Liu, J. Mu, and X. Li, "Experimental demonstration of using divergence cost-function in SPGD algorithm for coherent beam combining with tip/tilt control," *Opt. Exp.*, vol. 21, no. 21, pp. 25045–25055, Oct. 2013.

[5] X. Wang *et al.*, "350-W coherent beam combining of fiber amplifiers with tilt-tip and phase-locking control," *IEEE Photon. Technol. Lett.*, vol. 24, no. 19, pp. 1781–1784, Oct. 2012.

[6] M. A. Vorontsov, "Adaptive photonics phase-locked elements (APPLE): System architecture and wavefront control concept," *Proc. SPIE*, vol. 5895, 2005, Art. no. 589501.

[7] C. Wilcox, J. Andrews, S. Restaino, S. Teare, D. Payne, and S. Krishna, "Analysis of a combined tip-tilt and deformable mirror," *Opt. Lett.*, vol. 31, no. 6, pp. 679–681, 2006.

[8] P. Yang, R. Yang, F. Shen, X. Li, and W. Jiang, "Coherent combination of two ytterbium fiber amplifier based on an active segmented mirror," *Opt. Commun.*, vol. 282, no. 7, pp. 1349–1353, 2009.

[9] L. Beresnev and M. Vorontsov, "Design of adaptive fiber optics collimator for free-space communication laser transceiver," *Proc. SPIE*, vol. 5895, 2005, Art. no. 58950R.

[10] M. Vorontsov, T. Weyrauch, L. Beresnev, G. Carhart, L. Liu, and K. Aschenbach, "Adaptive array of phase-locked fiber collimators: Analysis and experimental demonstration," *IEEE J. Sel. Topics Quantum Electron.*, vol. 15, no. 2, pp. 269–280, Jan. 2009.

[11] L. Beresnev *et al.*, "Design of a noncooled fiber collimator for compact, high-efficiency fiber laser arrays," *App. Opt.*, vol. 56, no. 3, pp. B169–B178, Jan. 2017.

[12] C. Geng *et al.*, "1.5 kW incoherent beam combining of four fiber lasers using adaptive fiber-optics collimators," *IEEE Photon. Technol. Lett.*, vol. 25, no. 13, pp. 1286–1289, Jul. 2013.

[13] D. Zhi, P. Ma, Y. Ma, X. Wang, P. Zhou, and L. Si, "Novel adaptive fiber-optics collimator for coherent beam combination," *Opt. Exp.*, vol. 22, no. 25, pp. 31520–31528, Dec. 2014.
[14] T. Weyrauch *et al.*, "Deep turbulence effects mitigation with coherent combining of 21 laser beams over 7 km," *Opt. Lett.*, vol. 41, no. 4, pp. 840–843, Feb. 2016.
[15] F. Li, C. Geng, G. Huang, Y. Yang, X. Li, and Q. Qiu, "Experimental demonstration of coherent combining with tip/tilt control based on adaptive space-to-fiber laser beam coupling," *IEEE Photon. J.*, vol. 9, no. 2, Apr. 2017, Art. no. 7102812.
[16] J. W. Hardy, *Adaptive Optics for Astronomical Telescope*. New York, NY, USA: Oxford Univ. Press, 1998.
[17] G. Huang, C. Geng, F. Li, Y. Yang, and X. Li, "Adaptive SMF coupling based on precise-delayed SPGD algorithm and its application in free space optical communication," *IEEE Photon. J.*, vol. 10, no. 3, May 2018, Art. no. 7904212.
[18] M. Fan, L. Huang, M. Li, and C. Rao, "High-bandwidth control of piezoelectric steering mirror for suppression of laser beam jitter," *Acta. Phys. Sin.*, vol. 65, no. 2, 2016, Art. no. 024209.